ELSEVIER

Colloids and Surfaces
A: Physiochemical and Engineering Aspects 153 (1999) 255–270

COLLOIDS AND SURFACES A

Non-equilibrium particle morphology development in seeded emulsion polymerization. 1: penetration of monomer and radicals as a function of monomer feed rate during second stage polymerization

Jeffrey Stubbs[a], Ola Karlsson[a], Jan-Eric Jönsson[1,b], Eric Sundberg[2,a], Yvon Durant[a], Donald Sundberg[a,*]

[a] *Department of Chemical Engineering, Polymer Research Group, University of New Hampshire, Durham, NH 03824, USA*
[b] *Department of Chemical Engineering II, Lund Institute of Technology, PO Box 124, SE-22100 Lund, Sweden*

Abstract

Starve feeding of monomers is often used in an attempt to control latex particle morphology, especially when non-equilibrium structures are desired. For the case of a polar seed polymer and a non-polar second stage polymer, we have analyzed the relative probabilities of reaction and diffusion of polymer radicals and monomers as they penetrate the seed particle. The resultant penetration ratios (for polymer radicals and monomers) and fractional penetration values (depth of penetration) correlate well with a number of different non-equilibrium morphologies obtained from a wide variety of experimental reaction conditions. We conclude that the lack of polymer radical penetration is responsible for non-equilibrium core-shell structures for the glassy PMMA seed/PS system, while the styrene monomer easily penetrates the entire particle, even at very slow monomer feed rates. When the polar, low T_g PMA is substituted for the PMMA seed, the polymer radicals cannot be excluded from the particle center and an inverted core-shell equilibrium structure is obtained at all monomer feed rates.

Keywords: Latex; Morphology; Non-equilibrium; Diffusion; Core-shell

* Corresponding author. e-mail: dcs@christa.unh.edu
[1] Present address: Hoescht-Perstorp AB, SE-284 00 Perstrorp, Sweden.
[2] Present address: Department of Biochemistry, Molecular Biology and Cell Biology, Northwestern University, Evanston, IL, USA.

0927-7757/99/$ - see front matter
PII: S0927-7757(98)00449-X

1. Introduction

The applications of polymer latices often require that special attention be paid to the composite particle morphology. Consequently it has become of great interest to understand the interplay between the various parameters which control the morphology. Given the complexity of the many constituents of the typical latex formulation and reactor processing conditions, this is not a small task. Aside from the choice of monomers to be used, one often finds multiple surfactants and initiators in use, along with a variety of methods used to operate the latex reactor. The latter involve the use of different temperatures and monomer feeding patterns. Our objective over the past several years has been to develop quantitative guidelines and predictive methods for estimating the equilibrium morphology [1,2]. The purpose of this paper is to extend that work to consider non-equilibrium conditions and to comment particularly on those parameters thought to control the placement of the second stage polymer at the periphery of the particle so as to form a shell.

Among the formulation parameters considered to be important in controlling the particle morphology are surfactants [3,4], initiators [5,6], polymer type [7], and cross-linking of the seed polymer [8,9]. Cross-linking of the seed polymer creates elastic forces which compete with the interfacial forces in the control of morphology. The particle structure is very sensitive to the level of cross-linking, which can easily dominate morphology control [8,9]. The use of carboxylic acid co-monomers in either polymer stage can also lead to dramatic differences in morphology [10,11], but this has not been treated in a quantitative and predictive manner as far as we know.

The reaction temperature and method of monomer feeding during the second stage polymerization are also potentially important parameters in controlling the particle morphology. Temperature has an effect on the initiator dissociation rate, the polymerization rate coefficients and the internal viscosity of the particles during reaction. Such effects can influence the tendency for the conditions in the particle to deviate from thermodynamic equilibrium and to result in 'kinetically controlled' morphology. The monomer is most often fed to the reactor during the second stage polymerization in order to control the speed of the reaction and allow for good temperature control in commercial reactors. It may also influence the latex morphology by creating high-levels of viscosity in the particles (i.e. at very slow feed rates) and contribute to kinetically controlled particle structures. It should be noted that there are an infinite number of monomer feed rates possible, from infinitely fast (i.e. batch reaction) to infinitely slow. The so-called 'starve feed' rate occurs somewhere within this range. Clearly as the monomer is fed more and more slowly to the reactor, the monomer concentration within the particles is lower throughout the reaction. This affects the viscosity within the particle and the instantaneous reaction rate, both of which have an influence on the developing particle morphology. As one considers more and more deeply the local conditions within the particles during such a process, one becomes interested in the manner in which the monomer and polymeric free radicals (both originating in the aqueous phase) penetrate the particles during the reaction. Under the conditions that either the monomer or the radicals cannot penetrate to the center of the particle, the second stage polymer will not be formed within the unpenetrated region, although it may migrate there after it has been formed. Following this thought process leads one to conclude that there may be some monomer feed rate at which the monomer or polymeric radicals are excluded from nearly all of the seed particle, resulting in the classic core-shell (CS) particle. In the remainder of this paper we deal with the quantitative aspects of this thought.

2. Monomer and radical penetration during reaction

The investigated systems in the present study have either polar, glassy seed (PMMA) and a non-polar second stage (PS) or a polar non-glassy seed (PMA) and a non-polar second stage (PS). The equilibrium latex particle morphology in both these systems is expected to be an inverted core-

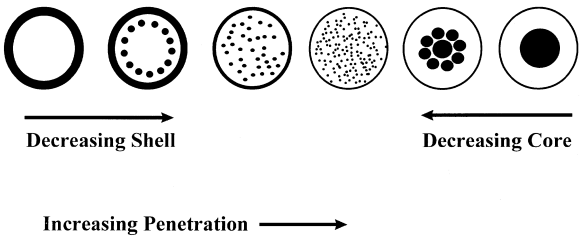

Fig. 1. Schematically drawn particle morphologies and second stage polymer penetration as expected from a polar seed and a non-polar second stage polymer. The light phase represents the seed polymer and the dark phase represents the second stage polymer.

shell (ICS) with the non-polar PS forming the core. The effect of the monomer feed rate, radical flux to the particles, the temperature of reaction and the particle size on latex particle morphology were studied.

The morphology expectations for the studied system, are presented in Fig. 1. The light phase in the particles represents the seed phase and the dark phase represents the second stage polymer. At the left part of the figure a core shell morphology is drawn, and moving to the right the morphologies shown have a decreasing polymer shell and an increasing amount of the second stage polymer in the particle cores. The inverted core shell morphology to the extreme right represents the equilibrium structure for the studied system and is the expected particle morphology if there are no kinetic restrictions for the newly formed second stage polymer.

The core shell morphology represents the situation where the internal particle viscosity may be high enough such that the penetration of the second stage polymer into the seed particle is restricted. Moving to the right in the figure also means that the internal particle viscosity is lowered during polymerization and the final particle morphologies get closer to the equilibrium as the second stage polymer penetration is increased.

When the monomer is charged to a reactor in a seeded polymerization, it has to diffuse through the aqueous phase and then across the water particle interphase and finally into the particles where it reacts. It is usually considered that in a batch reaction, the possible diffusion of the

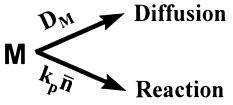

monomer within the particle is always much faster than the reaction. When the monomer is fed slowly to the latex, such may or may not be the case. A useful concept is to consider a monomer molecule somewhere within the latex particle and to consider the relative frequency for the molecule to diffuse or to react with a free radical, as shown below:

By defining a penetration ratio for the monomer, PR_M, as the quotient between the frequency for the monomer to diffuse divided by the frequency for the monomer to react it is possible to compute a useful number. If the PR_M is large the probability for diffusion is larger than the reaction; for a small PR_M the probability for the reaction is larger than for diffusion. The monomer penetration ratio is calculated as described in Eq. (1):

$$PR_M = (D_M/x^2)/(k_p \cdot [R\cdot]) \quad (1)$$

where D_M is the diffusion coefficient for the monomer assuming Fickian diffusion, x is the jump distance for a diffusive step, k_p is the rate coefficient for propagation and $[R\cdot]$ is the radical concentration. Although the diffusion in glassy polymers may not be accurately described by Fickian diffusion, but instead by anomalous or case II diffusion [12], it is considered sufficient for the purposes of these calculations. $[R\cdot]$ is expressed as:

$$[R\cdot] = \bar{n}/(V_p \cdot N_A) \quad (2)$$

where $\bar{n}$ is the number of radicals per particle, V_p is the particle volume and N_A is Avogadro's number. The final expression for the monomer penetration ratio then becomes:

$$PR_M = (D_M/x^2)/\left\{\left(k_p \cdot \bar{n}\right)/(V_p \cdot N_A)\right\} \quad (3)$$

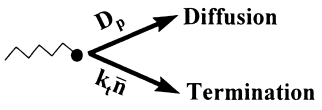

The second stage oligomeric radicals formed in the aqueous phase (i.e. we have assumed that a water soluble initiator is present) will be captured by the particles as they have reached a short length (two to three monomer units for styrene). A corresponding penetration ratio for the polymer radicals, PR_p, can also be defined. As shown below the PR_p, is defined as the quotient of the frequency for the polymer radicals to diffuse and the frequency for the radicals to terminate.

The radical penetration ratio is calculated as described in Eq. (4):

$$PR_p = \left(D_p/x^2\right)/(k_t \cdot [R\cdot]) \tag{4}$$

where D_p is the diffusion coefficient for the polymer radical, x is the jump distance for a diffuse step, k_t is the rate coefficient for termination and $[R\cdot]$ is the radical concentration expressed as in Eq. (2). The final expression for the polymer radial penetration ratio then becomes:

$$PR_p = \left(D_p/x^2\right)/\left\{(k_t \cdot \bar{n})/(V_p \cdot N_A)\right\} \tag{5}$$

It has been suggested [13–18] that in a glassy polymer at the low monomer concentrations typical of a slow feed of the second stage monomer, the diffusion coefficient of a polymer chain scales with the inverse of the square of the number of repeating units. By considering that the diffusion of a radical chain end is the sum of the center of mass and reaction diffusion contributions, i.e. movement of the chain end by propagation [19], the overall diffusion coefficient for a radical of i number of repeating units can be written as:

$$D_p = D_i^{\mathrm{com}} + D^{\mathrm{rd}} \tag{6}$$

where D_i^{com}, the coefficient for center of mass diffusion, is given by

$$D_i^{\mathrm{com}} = D_M(w_p)/i^2 \tag{7}$$

and $D_M(w_p)$ is the diffusion coefficient of the monomer in a seed latex with a polymer weight fraction of w_p. Figure 1 in Mills et al. [13] was used as a guide to determine values of $D_M(w_p)$ as presented in Fig. 2. These values need to be corrected for the reaction temperatures used in experiments of interest. $D_M(w_p)$ is very sensitive to monomer concentration, especially near the glass transition region. This will be discussed more fully later [20]. D^{rd}, the coefficient for reaction diffusion, is given by [17]:

$$D^{\mathrm{rd}} = (1/6)k_p[M]a^2 \tag{8}$$

where $[M]$ is the concentration of the monomer in the particles and 'a' is the root-mean-square end-to-end distance per square root of the number of monomer units in a polymer chain, i.e. 'a' is the mean distance moved, in a random flight sense, at each propagation step. The rate coefficient k_p [17] is determined as:

$$1/k_p = 1/k_p^{\mathrm{chem}} + 1/k_p^{\mathrm{diff}} \tag{9}$$

where k_p^{chem} is the chemically controlled propagation rate constant and k_p^{diff} is the diffusion controlled propagation rate constant defined as [17]:

$$k_p^{\mathrm{diff}} = 4\pi N_A\left(D_M(w_p) + 1/6k_p[M]a^2\right)\sigma \tag{10}$$

where σ is the Lennard–Jones (van der Waals) radius of a monomer unit. Combining Eq. (9) and Eq. (10) allows k_p^{diff} and k_p to be calculated. At high w_p it is only the monomer that undergoes any significant center-of-mass diffusion, and the reaction–diffusion coefficient of the growing chain will to an increasing extent affect the k_p as the w_p gets higher. The propagation becomes diffusion-controlled at w_p over approx. 0.8 in glassy polymers and the k_p starts to decrease at higher values.

Most semi-batch emulsion polymerizations are performed at w_p higher than 0.8 and k_p may therefore be affected. During those conditions with particle sizes in the order of 0.5 μm, low monomer concentrations in the particles, and a

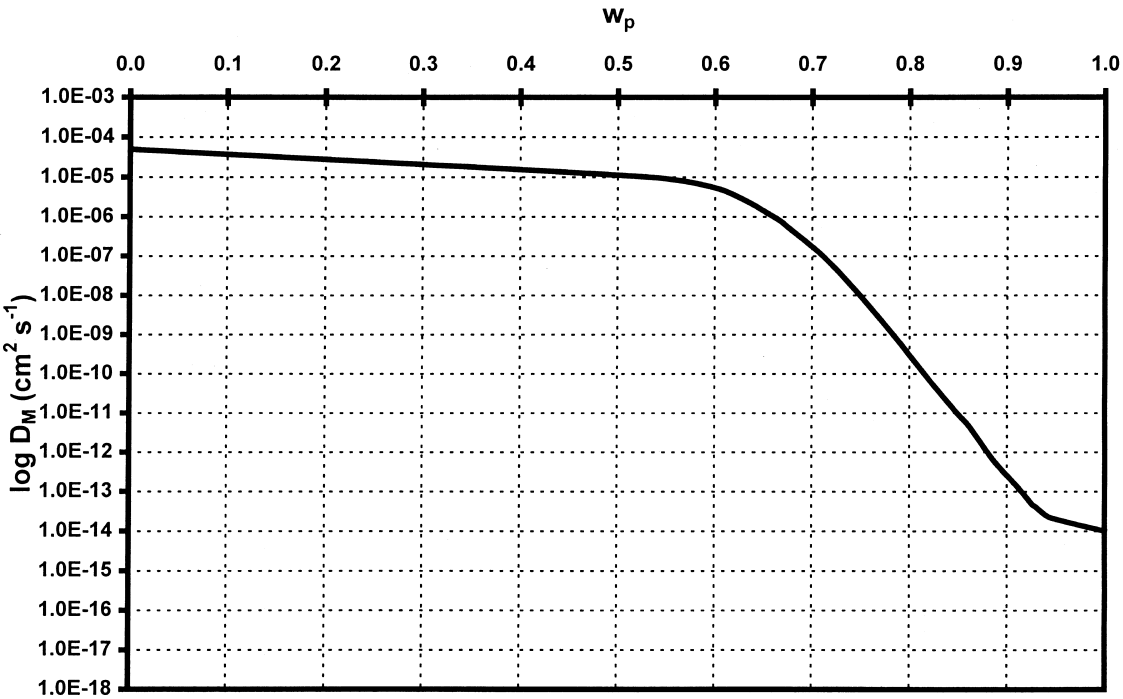

Fig. 2. Diffusion coefficients of small penetrations in PMMA around 50°C [13].

low k_p, we still find relatively high-rates of polymerization. Thus there is a large deviation from The ideal Smith and Ewart case II. The number of radicals in many of the investigated systems in this work is over 50, and in some systems substantially more.

Also the termination reaction is influenced by the internal particle viscosity. At conversions up to approx. 0.3 the termination reaction conforms to conventional kinetics. At higher conversions the entanglements of polymer molecules and the decreasing free volume reduces the termination rate. During this stage the termination reaction is chain length dependent. At conversions above approx. 0.8 [17] the termination rate is further reduced by reaction diffusion, which is independent of chain length. In the present study the k_t used at high-conversions was calculated according to the method developed by Soh [21] as presented in Eq. (11):

$$k_t^{\text{diff}} = k_t^0 / r \tag{12}$$

where k_t^{diff} is the diffusion controlled termination rate coefficient used at w_p over 0.6, k_t^0 is the termination rate constant at low conversions and 'r' is a reduction factor for the termination reaction. In the present study the conversions are always higher than 0.6, which makes Eq. (11) useful in the calculations. The reduction factor is taken from Soh's [21] work, and it is due to a combination of the entanglements of large molecules and the reaction diffusion.

2.1. Fractional penetration calculations

One limitation with defining a penetration ratio for an entering radical is that of defining a single value for the diffusion coefficient. This is because the radical is continually growing via propagation and, as it does, the diffusion coefficient decreases markedly. It may be more insightful to look at the penetration of polymeric radicals in a more dynamic way, taking into account this decrease in

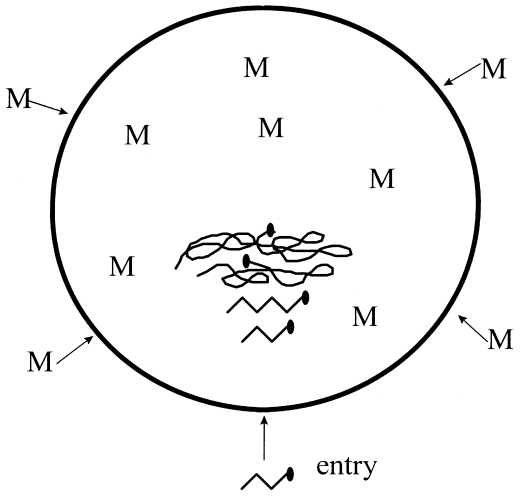

Fig. 3. Schematic representation of the simultaneous diffusion and growth of a polymeric radical within a latex particle.

diffusivity as the radical chain length increases with each propagation step. This is depicted in Fig. 3.

The following method has been developed to give an approximation of how far, on average, an entering radical can penetrate into a particle before undergoing termination. The distance, Δx, that a radical chain end can move in a given time, Δt, was calculated by the simple form of Fick's law as:

$$\Delta x = (D_p \Delta t)^{1/2} \tag{12}$$

The dynamic simulation starts with an oligomeric radical with chain length z at the surface of the particle. The value of z is dependent on the type of second stage monomer and is usually considered to be within the range of two to 10 [22] repeating units. Once in the particle, the radical chain length is increased by one unit for each time interval equal to $1/(k_p[M])$, the average time between propagation steps. The diffusion coefficient is then calculated from Eqs. (6)–(8) and the distance for each step by Eq. (12). The total time that the simulation is carried out is equal to $1/(k_t[R\cdot])$, the average lifetime of a radical. The results can be shown as graphs of fractional penetration (i.e. distance divided by particle radius) vs. time. Such a plot is shown in Fig. 4 where the initial rate at which the radical penetrates is relatively fast and then as the chain grows, the rate slows down and reaches a steady value. The initial rapid penetration is a result of center of mass diffusion of the short polymer radical. As the chain grows it begins to become entangled and then the center of mass diffusion term becomes negligible and the movement of the radical chain end becomes controlled by reaction diffusion. For glassy seed polymers with a slow monomer feed rate, the concentration of the monomer is so small that the movement of the radical is always controlled by reaction diffusion, and center of mass diffusion is a minor factor. The subject of many reports in the literature is the ongoing debate as to whether charged radicals can diffuse freely inside the latex particles or whether they are anchored to the particle surface [13,22–26]. It is interesting to note that if the radicals are considered to be tethered to the surface, then there may be no significant difference between a soft seed and a glassy seed because both cases may be controlled by reaction diffusion, and that the variable that could increase or decrease the diffusion coefficient is the monomer concentration by increasing reaction diffusion.

3. Experimental

3.1. Chemicals

Styrene and methyl methacrylate monomers (Aldrich) and methyl acrylate (Acros Organics) were vacuum distilled to remove the inhibitor and

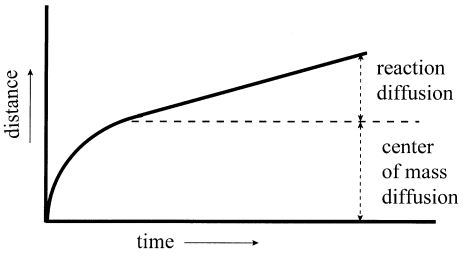

Fig. 4. Typical behavior for the penetration of a growing polymeric radical into a latex particle as a function of time.

stored at −10°C. Potassium persulfate (analytical grade, Acros Organics, Merck) was used for all experiments. Analytical grade sodium bicarbonate (EM Science) was used as the buffer. Methyl methacrylate and styrene (Merck) used in experiments performed in Lund were freed of the inhibitor by passing the monomers through a column filled with active basic aluminum oxide (Merck) and stored at 8°C.

3.2. Seed latex preparation

The PMMA and PMA seeds were prepared by surfactant free, batch emulsion polymerization with potassium persulfate as initiator. The PMA seed was polymerized at 70°C and the PMMA seed at 80°C. The PMMA seed used in Lund was polymerized at 70°C. The water and sodium bicarbonate were charged to the reactor and degassed with nitrogen to remove oxygen. The monomer was added to the reactor and brought up to the reaction temperature and potassium persulfate was added. Conversion was monitored by gravimetry. Particle size for the PMMA (ejs-015) seed was calculated by turbidity measurements. Particle sizes for the PMA latex was measured by quasi-elastic light scattering (QELS) using a Coulter® Nanosizer™. For the PMMA seed used in Lund the unreacted initiator was removed from the latex using a Dowex 2×8 OH^- ion-exchange column. Solid content was determined after ion-exchange and particle sizes were measured by QELS using a Coulter N4 MD. Data for the seed latices are contained in Table 1.

Table 1
Seed latex polymerizations

Seed name	ejs-15	jS1	jS2	jS3	jmsII-43
Water (g)	1079.8				905
MMA (g)	113.9				–
MA (g)	–	–	–	–	95
$NaHCO_3$ (g)	0.198				0.165
KPS (g)	0.633				0.535
Temp (°C)	80	70	70	70	70
Diameter (nm)	250[a]	510	560	480	440
% Solids	8.8	15.75	4.68	17.13	6.5

[a] Denotes particle size by turbidity measurements, others by QELS.

3.3. Second stage polymerizations

Second stage polymerizations of styrene using PMMA seeds were performed at 60°C. Polymerizations with PMA seed were done at 70°C. Experiments at UNH used a stage ratio of styrene to seed polymer of 200% in all cases. Batch reactions were conducted both with and without a monomer swelling period. For the pre-swelled experiments the monomer was added to the latex and allowed to swell into the seed particles for 2 h at room temperature. For the non-swelled batch reactions, all of the monomer was added to the seed latex at the very beginning of the reaction. For the monomer fed reactions, the monomer was added at a controlled rate using a motor driven glass syringe. Additional DI water was to control the final solid content. The water, seed latex and buffer were added to the reactor and degassed with nitrogen to remove dissolved oxygen. Potassium persulfate was then added and the styrene feed started. Conversion was monitored by gravimetry.

The styrene polymerizations with PMMA seed performed in Lund were done in a 200-ml calorimetric reactor at 60°C and 100% stage ratio [24,27]. The seed latex, sodium dodecyl sulfate, ascorbic acid and vanadium (IV) oxide sulfate were charged to the reactor. Vanadium (IV) oxide sulfate and ascorbic acid were part of the redox initiator system used in these reactions in order to effect precise control over the rate of radical production. Initiator solutions of KPS in water were continuously fed to the reactor at a constant rate of 1×10^{-7} mol min^{-1}. The styrene monomer was fed to the reactor at various rates.

3.4. Transmission electron microscopy (TEM)

The PMMA/PS latices were embedded in epoxy and microtomed sections were prepared. For the PMA/PS latices, microtomed sections were not used as the PMA smeared during the microtoming. Instead, the whole particles were observed by drying the diluted latex on copper TEM grids coated with nitrocellulose. Samples were stained with ruthenium vapor and observed in a Hitachi H600 transmission electron micros-

cope. Latex samples made in Lund were examined without staining in a JEOL 100U transmission electron microscope.

4. Results and discussion

In this section we discuss the application of the penetration ratios and the fractional penetration calculations to all of the experiments shown in Table 2a,b. Detailed calculations for PR_M and PR_p are shown in Appendix A for experiment J3B described in Table 2b. All other values are included in Table 3 which appears later.

That the effect of monomer feed rate on particle morphology can be dramatic in systems with glassy seed polymers is shown in Fig. 5a,b. The microtomed particles shown in the transmission electron microscope micrographs in Fig. 5a are from a batch reaction in which the styrene monomer was allowed to swell into the PMMA seed particles for several hours before the start of the reaction. Those in Fig. 5b are from the same experiment without allowing for any swelling time (i.e. all of the monomer was added at one time to the seed latex just after the initiator was added). It is obvious that in the latter case the polystyrene (PS), stained by ruthenium tetraoxide, has not penetrated the unstained PMMA nearly as much as in the former case. This being the case it was interesting to control the monomer feed rate to the seed latex to varying degrees in order to observe its effect on the particle morphology. Fig. 6a–c shows the results of slower and slower feed rates of the styrene monomer with all other conditions held constant. The gravimetric analysis of latex samples withdrawn at various times during the reaction allowed us to calculate the monomer level in the particles at any time and also to determine the reaction rate. Given the formulation details we could then compute the apparent

Table 2
(a) Second stage polymerization conditions

Experiment name Seed name	ejs-17 ejs-15	ejs-18 ejs-15	ejs-20 ejs-15	JMS-49 jms-43	ejs-16 ejs-15	ejs-27 ejs-15
Seed latex (g)	94.7	94.7	94.7	150.04	94.7	85.2
Water (g)	38.7	39.6	38.2	195.35	37.2	32.7
Styrene (g)	18	18	18	19.5	18	16.2
$NaHCO_3$ (g)	0.0193	0.0155	0.0155	0.075	0.0164	0.0148
KPS (g)	0.0778	0.0748	0.076	0.0797	0.0752	0.0691
Temp (°C)	60	60	60	70	60	60
Monomer feed rate (ml h^{-1})	23.9	11.9	53	8.6	Batch, no swelling	Batch, swelled
Monomer feed time (min)	50	100	225	150		
Particle size (nm)				590		
Solid content	16.2	16.2	16.3	7.2	15.7	16.45

(b) Second stage conditions (Lund)

Experiment name Seed name	J2C jS1	J2D jS2	J3A jS3	J3B jS3	J3C jS3	J3D jS3
Seed latex (g)	80	100	80	80	80	80
Styrene (g)	10.91	4.64	14.2	14.2	14.2	14.2
SDS (g)	0.15	0.11	0.15	0.15	0.15	0.15
Ascorbic acid (g)	0.3	0.3	0.3	0.3	0.3	0.3
$VOSO_4$ (mg)	5.0	5.0	5.5	5.5	5.5	5.5
KPS feed rate (mol min^{-1})	1×10^{-7}	1×10^{-7}	1×10^{-7}	1×10^{-7}	1×10^{-7}	1×10^{-6}
Temp (°C)	60	60	60	60	60	60
Monomer feed rate (ml h^{-1})	3.0	3.0	1.8	3.0	6.0	6.0
Monomer feed time (min)	240	102	520	312	156	156

Table 3
Calculated penetration parameters and experimental conditions

Experiment	Seed	$[M]$	$\bar{n}$	PR_M	PR_{rad}	Fractional penetration	Morphology
EJS-17	PMMA	2.56	72	6.9E + 11	275 454	28	Type 2
EJS-18	PMMA	1.53	57	8.4E + 07	58	0.60	Type 1
EJS-20	PMMA	1.12	38	3.3E + 06	20	0.58	Type 1
J2C	PMMA	0.45	6209	7.5E + 03	10.00	0.15	Type 0
J2D	PMMA	1.10	488	1.7E + 06	16 171	3.50	Type 2–3
J3A	PMMA	0.76	221	2.8E + 04	9.0	0.10	Type 0
J3B	PMMA	1.36	72	2.6E + 07	126	0.85	Type 1
J3C	PMMA	1.63	109	3.0E + 06	357	0.80	Type 2
J3D	PMMA	0.81	564	5.4E + 04	5	0.03	Type 0
JMS2-49	PMA	3.32	67	1.0E + 13	3 192 066	15	Type 5

radical concentration in the particles and make the penetration ratio and fractional penetration calculations. Table 3 lists the results for all of the experiments described in this work, including values for the instantaneous monomer concentration and number of radicals within the particles, and the penetration ratios for both the monomer and polymer radicals. For the experiments shown in Fig. 6 the penetration ratios for the monomer are all in the 10^8–10^{11} range, indicating that the monomer readily diffuses within the particle. Thus we expect no monomer gradient in these particles. The penetration ratios for the polymer radicals, on the other hand, vary from high values (approx. 275 000) at high-rates of monomer addition (Fig. 6a) to much lower values (approx. 50) at much slower monomer addition rates (Fig. 6b,c). As is seen from the electron microphotographs in Fig. 6 the particle morphologies exhibit less and less penetration of the second stage PS with slower monomer feed rates, consistent with lowering penetration ratios. Thus it appears that limitations on polymer radical transport may be the cause for these non-equilibrium structures, and not limitations on the monomer transport. This is consistent with the conclusions of Jönsson et al. in earlier papers [24,27].

Calculated results for the fractional penetration of polymer radicals have also been done for all of the experiments, and these results are displayed in Table 3. Those applicable to the experiments in Fig. 6 show decreasing fractional penetration (28, 0.6 and 0.6, respectively) with slower monomer feed rates. This indicates that from this perspective the polymer radicals appear to have the ability to either reach the center of the particle or significantly penetrate during the reaction and thus we may expect to find a second stage polymer throughout the particle. The micrographs actually show that while there is a PS shell formed in each instance, there are occlusions of PS reaching the center of the particle at the most rapid monomer feed rate (Fig. 6a), but fewer or no occlusions in the particle center at the slower feed rates (Fig. 6b,c).

Jönsson [24,27] has reported the morphology results for a variety of reaction conditions for the same PMMA seed–PS second stage system discussed above. In this work a reaction calorimeter was used and very good knowledge of the instantaneous monomer concentrations within the particles was obtainable. This is quite important for some reaction conditions as the diffusion coefficients are highly dependent upon the local monomer concentration. The series of experiments designated J3A–J3D described in Table 2b are useful to discuss in the context of monomer and polymer radical penetration and resultant particle morphology. The PMMA seed latex particle size was rather large at 510 nm, but this allowed for good resolution in the electron micrographs. In experiments J3A–J3C the monomer

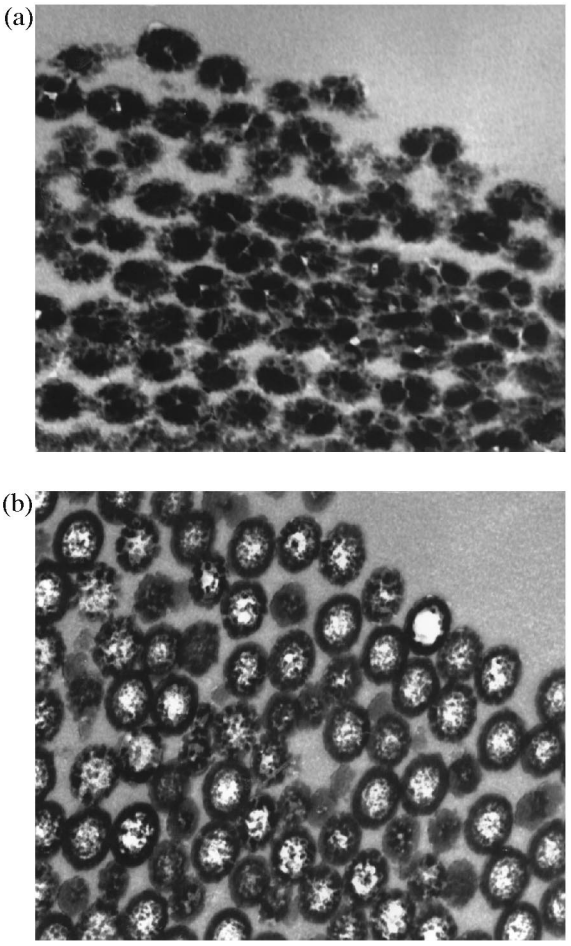

Fig. 5. TEM micrographs showing structured latex particles made from the PMMA seed and styrene as the second stage. In the micrographs styrene is represented by the dark phase. (a) Preswelled batch reaction; (b) unswelled batch reaction.

feed time was varied from 520 min down to 156 min at the same radical flux to the particles. This accounted for instantaneous monomer concentrations in the range of 0.8–1.6 M (0.92–0.83 weight fraction polymer) and, as seen in Table 3 variations in the monomeric diffusion coefficient of approximately three orders of magnitude. Again, the penetration ratios for the monomer are all very large, while those for the polymer radicals vary between nine and 357 with increasing monomer feed rate. The corresponding fractional penetrations varied from 0.10 to 0.80. At the slowest feed rate ($PR_p = 9$ and fractional penetration = 0.10), the morphology for J3A as shown in Fig. 7a is very clearly a core-shell with no identifiable PS in the core of the particle. When the feed rate was increased such that the instantaneous monomer concentration was 1.4 M ($PR_p = 126$ and fractional penetration = 0.85), the particle consisted of a shell of PS with occlusions in the core, as shown for experiment J3B in Fig. 7b. Similar results were obtained for J3C shown in Fig. 7c. Here the polymer radical penetration ratio was calculated to be 357 and the fractional penetration was 0.80. In this particular experiment the monomer concentration in the particles was substantially higher at the end of the monomer feed than near the beginning, indicating unsteady state conditions during the experiment. Our calculations were done for those conditions at the end of the feed period. Experiment J3D provides an interesting situation in which the monomer feed rate is the same as in J3C, but the radical flux to the particle is 10 times higher. This increased the number of radicals in the particle and lowered the monomer concentration from 1.6 to 0.8 M, with the result that PR_p decreased from 357 to five and the fractional penetration decreased from 0.80 to 0.03. The morphology was clearly CS, as shown in Fig. 7d. These experimental results demonstrate the interplay between monomer feed rate and radical flux in determining the conditions which control the non-equilibrium morphology. The penetration ratio and fractional penetration values for the polymer radicals are sensitive to both variables and correlate well with the observed morphology.

An additional set of experiments described earlier by Jönsson et al. [24] have also been analyzed in the present work. These two experiments are designated as J2C and J2D in Table 2b. During the second stage reactions the monomer feed rate per particle was significantly higher in J2D than in J2C. This resulted in a significant difference in the instantaneous monomer concentrations, and the penetration ratios of the polymer radicals were calculated to be 10 and 16 171, respectively. Fig. 8a very clearly shows CS particles for J2C and Fig. 8b shows PS penetration for J2D. The fractional penetration values for the two experiments are 0.15 and 3.50, respectively. Combined,

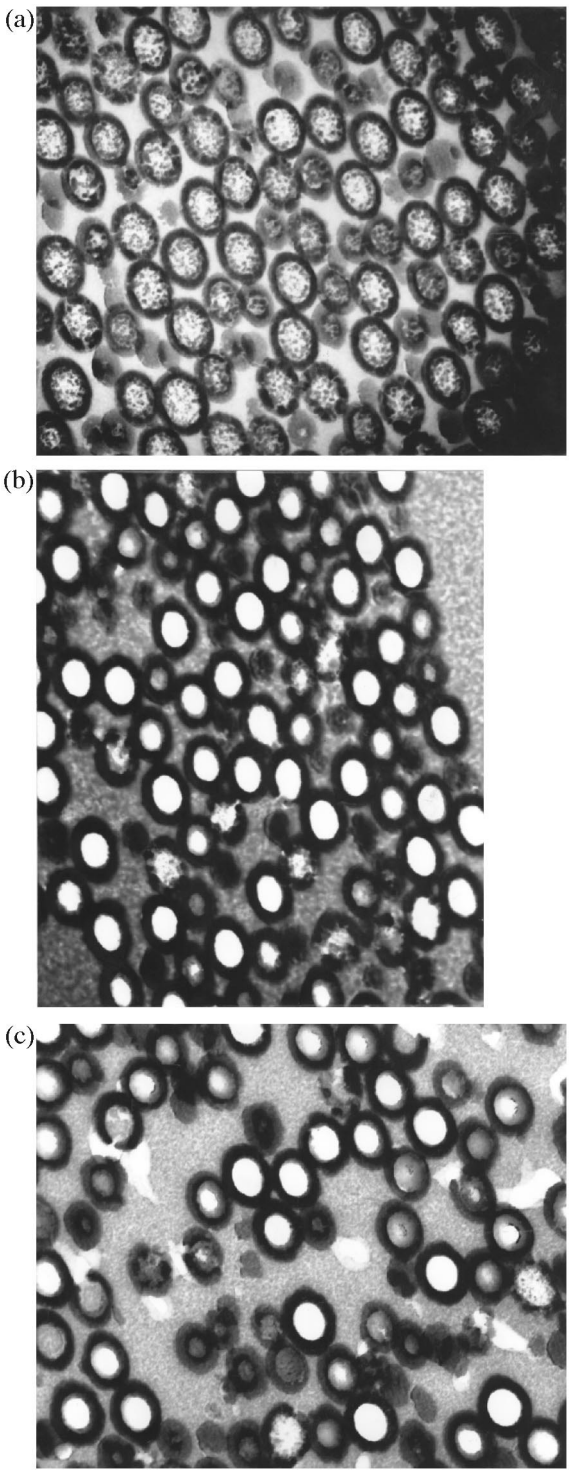

Fig. 6.

the experimental results correlate well with the computations.

All of the above experiments utilized a glassy, polar seed polymer. At low monomer concentrations in such particles, the polymer radical penetration can obviously be restricted, leading to CS structures even when the shell polymer is much less polar than the core polymer. It is of further interest to consider the effect of significantly changing the T_g of the seed polymer while retaining its polar nature. Thus we have produced a seed polymer of PMA at 440 nm particle size which is well above its glass point ($T = 14$°C) at the reaction temperature of 70°C. This situation should conceptually provide for easier polymer radical diffusion at low monomer concentrations than the glassy seed. Styrene monomer was fed to the PMA latex over a range of time periods, and the conditions for the case of a 375-min feed period is described in Table 2a. The results of the experiment and the calculations for penetration values are shown in Table 3. The polymer radical penetration ratio was very high at approx. 3 200 000 and the fractional penetration was 15.0, indicating that the polymer radicals should easily reach the center of the particle during the reaction. Fig. 9 shows a TEM photo for the composite particle stained with ruthenium tetraoxide. This photo displays whole particles, not microtomed sections as in the previous figures. Without a cryomicrotome we were unable to prepare sections without smearing the slices. However, it is quite clear that the stained PS has accumulated in the core of the particle, with the unstained PMA in the shell. All of the experiments at various monomer feed rates, including the batch reaction, displayed the same inverted CS morphology and are not shown for sake of brevity. The latices from this experimental series were all film forming at room temperature, providing further evidence that the PMA formed the shell of

Fig. 6. TEM micrographs showing structured latex particles made from the PMMA seed and styrene fed over time as the second stage monomer. In the micrographs styrene is represented by the dark phase. (a) EJS 017; (b) EJS 018; (c) EJS 020.

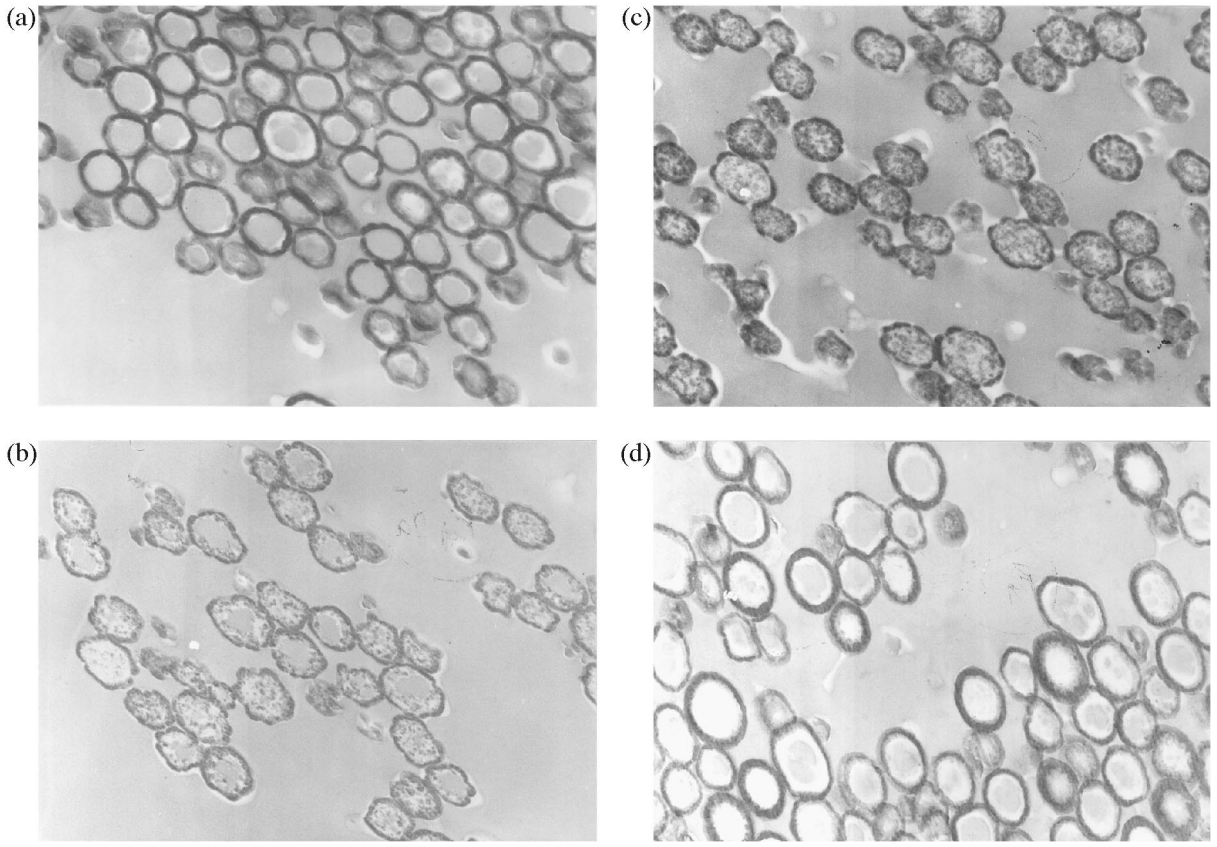

Fig. 7. TEM micrographs showing structured latex particles made from PMMA seed and styrene fed over time as second stage monomer. In the micrographs styrene is represented by the dark phase. (a) J3A; (b) J3B; (c) J3C; (d) J3D.

the particles. Thus it appears that these latices have all achieved their equilibrium morphology despite great differences in monomer feed rate.

At this point we find it useful to suggest that the penetration ratios and fractional penetration values can be correlated with the various particle structures shown in Fig. 1. This was accomplished by observing all of the TEM results for the experiments described in Table 2 and aligning the specific experiments (identified with the codes, such as J2C, etc.) with one of the morphologies shown in Fig. 1. After that we simply added the penetration ratios and fractional penetration values to create a new table as shown in Table 4. Based on these approximate placements we assigned order of magnitude values to the penetration ratios and correlated each with a particular morphology, as shown in the top row. For our own convenience we have used the log of the assigned PR_p values to indicate a 'type', or category of particle structure. Here Type 0 is a CS and Type 5 is an inverted CS, with Types 1–4 representing various non-fully phase separated particles. As this figure only applies to polar seed polymer and non-polar second stage polymer, all of the particles shown are non-equilibrium structures except for Type 5, the inverted CS. Given the approximate nature of the calculations and the great sensitivity of the diffusion coefficients to the instantaneous monomer concentration, we find the perspective offered from Table 4 to be useful to our assessment of the effects of several interrelated experimental variables on the non-equilibrium morphologies of the resultant latices. With further experiments and more detailed considerations of the diffusivity of the monomer and

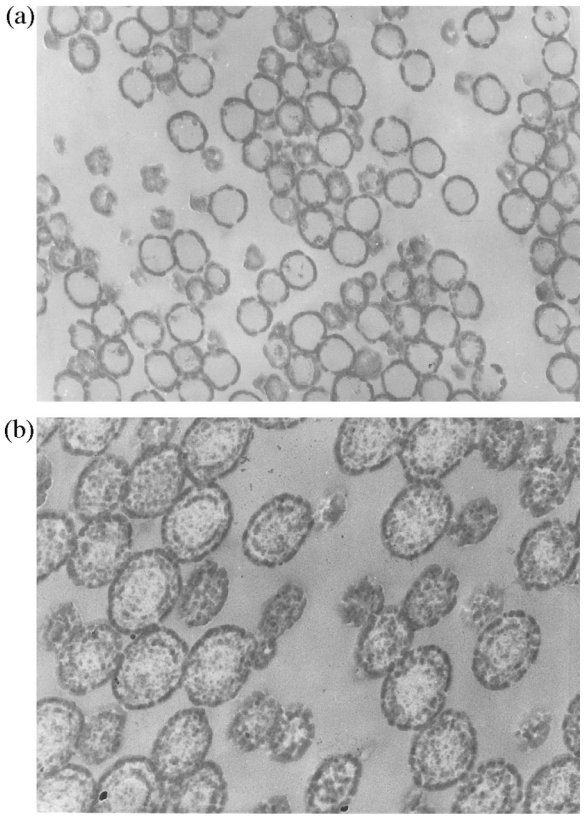

Fig. 8. TEM micrographs showing structured latex particles made from the PMMA seed and styrene fed over time as the second stage monomer. In the micrographs styrene is represented by the dark phase. (a) J2C; (b) J2D.

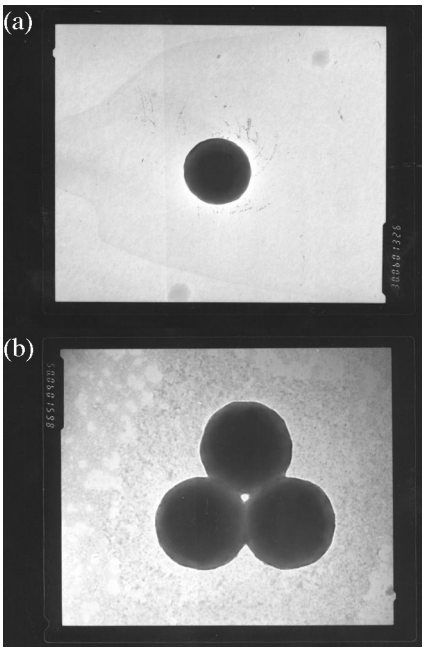

Fig. 9. TEM micrographs showing structured latex particles made from the PMA seed and styrene fed over time as the second stage monomer. In the micrographs styrene is represented by the dark phase. (a) JMSII-49; (b) Styrene fed over 375 min. No calculations made for this experiment. Picture included for further evidence of ICS morphology in the PMA/PS systems

polymer within latex particles we hope to further refine this table and its usefulness.

5. Concluding remarks

In this work we have tried to interpret the effects of a number of experimental variables on the final latex morphology through a simple assessment of probabilities for diffusion and reaction of both polymer radicals and monomers within the latex particle. It is concluded from this work that the monomer easily penetrates the latex particle in a manner that likely results in a uniform concentration profile across the particle, even during slow feeding of the monomer and even for seed polymers that are glassy. On the other hand, we conclude that polymer radicals may be restricted to the periphery of the particles when the radical flux is high enough and the monomer feed is slow enough for glassy seed polymers, but probably not for low T_g seed polymers. Given this viewpoint, we suggest that the term 'starve feeding' be refined to apply to those conditions for which the core of the particle is actually 'starved' for a reactive component, which in all cases we studied is the polymer radical and

Table 4
Correlation of penetration ratio with morphology

PR_P	1	10	100	1000	10 000	100 000
$\log_{10}(PR_P)$	0	1	2	3	4	5
Experiments	J2C J3A J3D	EJS18 EJS20 J3B	EJS17 J2D J3C			JMS2-49
Calculated PR_P	10 9.0 5.0	58 20 126	275 454 16 171 375			3 192 066
Calculated fractional penetration	0.15 0.10 0.03	0.60 0.58 0.85	28.0 3.5 0.8			15.0

not the monomer. Thus, for identical reaction conditions, the use of glassy seed polymers may result in a 'starve feed' process while the use of a low T_g seed is unlikely to produce such conditions. Clearly the tendency to produce non-equilibrium morphologies is much higher in the former case than in the latter case.

One of the obvious limitations to the analysis presented here is that we have only considered the properties of the seed polymer in describing the probabilities of diffusion and reaction, and only for a steady state reaction process. In the future it is necessary to consider the difference between glassy and soft second stage polymers, and to deal with reactions in which the instantaneous monomer concentration may not be constant with time. This is left to further work.

Nomenclature

a	Root mean square end-to-end distance per square root of the monomer units in a chain	(Å)
D_M	Diffusion coefficient for the monomer	($cm^2\ s^{-1}$)
D_p	Diffusion coefficient for the polymeric radical	($cm^2\ s^{-1}$)
D_i^{com}	Coefficient for center of mass diffusion	($cm^2\ s^{-1}$)
D^{rd}	Coefficient for reaction diffusion	($cm^2\ s^{-1}$)
$D_M(w_p)$	Diffusion coefficient of monomer in a seed with a polymer concentration of w_p	($cm^2\ s^{-1}$)
Δx	Distance of radical movement	
Δt	Time step in simulation	
i	Number of repeating units	
k_p	Rate coefficient for propagation	($dm^3\ mol^{-1}\ s$)
k_p^{chem}	Chemically controlled propagation rate constant	($dm^3\ mol^{-1}\ s$)
k_p^{diff}	Diffusion controlled propagation rate constant	($dm^3\ mol^{-1}\ s$)
k_t	Rate coefficient for termination	($dm^3\ mol^{-1}\ s$)
k_t^{diff}	Reaction controlled termination rate constant	($dm^3\ mol^{-1}\ s$)
k_t^0	Termination rate constant at low conversions	($dm^3\ mol^{-1}\ s$)
$[M]$	Concentration of monomer in the particles	($mol\ l^{-1}$)
N_A	Avogadro's number	(mol^{-1})
$\bar{n}$	Number of radicals per particle	
PR_p	Penetration ratio for polymeric radicals	
PR_M	Penetration ratio for the monomer	
r	Reduction factor for the termination reaction	
$[R\cdot]$	Radical concentration	($mol\ l^{-1}$)
σ	Lennard–Jones (van der Waals) radius of a monomer unit	(Å)
V_p	Particle volume	(dm^3)
w_p	Weight fraction polymer	
x	Jump distance for a diffusion step	(Å)

Acknowledgements

We are thankful for financial support from the University of New Hampshire Latex Morphology Industrial Consortium (BASF, DSM Research, Elf Atochem, ICI Paints, Mitsubishi Chemical, Wacker-Chemie, Zeneca Resins), the Swedish Foundation for International Cooperation in Research and Higher Education (STINT) for O. Karlsson, and for TEM photographs from Chemical Engineering II, Lund University, Sweden.

Appendix A: Sample calculations

The following sample calculation is provided for experiment J3B for conditions prevalent at the end of the monomer feed period. The volume of the particle, V_p, was determined from monomer feed conditions and the seed particle volume. The monomer concentration in the particles, $[M]$, was determined from conversion data [27]. In order to calculate the propagation rate coefficient, k_p, from (Eq. (9)), the value for the diffusion controlled propagation rate constant is required. Calculation of k_p and k_p^{diff} was accomplished by simultaneous solution of Eqs. (9) and (10), using the value for the chemically controlled propagation rate constant, k_p^{chem}, given in table A1:

$$k_p^{diff} = 17963.8\ l\ mol^{-1}\ s^{-1}$$

$k_p = 174.3\ \mathrm{l\ mol^{-1} s^{-1}}$

The average number of radicals per particle was calculated from the rate equation:

$$R_p = k_p[M]\,\bar{n}\,N_c/N_A$$

where R_p is the rate of polymerization, N_c is the particle concentration, and N_A is Avagadro's number, using rate data obtained from the calorimetric reactor:

$\bar{n} = 72$

The value for the termination rate constant, k_t, was calculated using Eq. (11) following the method outlined by Soh [21] as described previously, giving:

$k_t = 5.61 \times 10^5\ \mathrm{l\ mol^{-1}\ s^{-1}}$

The penetration ratio for monomer, PR_M, could then be calculated from Eq. (3), using the value of $D_m(w_p)$ given in Table A1:

$PR_M = 6.65 \times 10^7$

In order to determine the penetration ratio for polymeric radicals, a value for the diffusion coefficient of a polymer chain, D_p, was required. This was calculated from Eq. (6) with the center of mass diffusion coefficient, D_i^{com} from Eq. (7) and the coefficient for reaction diffusion, D^{rd}, from Eq. (8). For the sake of consistency in defining the penetration ratio for a polymeric radical, the value for the number of repeating units in the radical chain, i, was taken as being equal to 20. The values obtained are:

$$D_i^{\mathrm{com}} = 9.85 \times 10^{-14}\ \mathrm{cm^2\ s^{-1}}$$

$$D^{\mathrm{rd}} = 1.421 \times 10^{-13}\ \mathrm{cm^2\ s^{-1}}$$

$$D_p = 2.405 \times 10^{-13}\ \mathrm{cm^2\ s^{-1}}$$

The penetration ratio for the polymer, PR_p, was then calculated using Eq. (5):

$PR_p = 126$

Values for the individual parameters used in these calculations are listed in Table A1.

Table A1: values used for calculations for experiment J3B

V_p (l)	1.265×10^{-16}
$[M]$ (mol l^{-1})	1.358
w_p	0.86
k_p^{chem} (l mol^{-1} s^{-1}) [28]	176
$D_m(w_p)$ (cm^2 s^{-1})	3.94×10^{-11}
k_t^0 (l mol^{-1} s^{-1}) [21]	4.33×10^7
r [21]	77
x (Å)	6
a (Å)	6

References

[1] Y.G. Durant, D.C. Sundberg, Macromol. Symp. 92 (1995) 43.
[2] Y.G. Durant, D.C. Sundberg, ACS Symposium Series., No. 663, Washington, D.C., 1997, p. 44.
[3] D.C. Sundberg, A.P. Casacca, J. Pantazopoulos, M.R. Muscato, B. Kronberg, J. Berg, J. Appl. Polym. Sci. 41 (1990) 1425.
[4] Y.C. Chen, V. Dimonie, M.S. El-Aasser, J. Appl. Polym. Sci. 45 (1992) 487.
[5] I. Cho, K.-W. Lee, J. Appl. Polym. Sci. 30 (1985) 1903.
[6] S. Lee, A. Rudin, J. Polym. Sci.: Part A: Polym. Chem. 30 (1992) 2211.
[7] E.J. Sundberg, D.C. Sundberg, J. Appl. Polym. Sci. 47 (1993) 1277.
[8] Y.G. Durant, E.J. Sundberg, D.C. Sundberg, Macromolecules 29 (1996) 8466.
[9] Y.G. Durant, E.J. Sundberg, D.C. Sundberg, Macromolecules 30 (1997) 1028.
[10] O. Karlsson, H. Hassander, B. Wesslen, J. Appl. Polym. Sci. 63 (1997) 1543.
[11] O. Karlsson, Heterogeneous Film-Forming Latexes. Preparation — Morphology — Mechanical Properties, Doctoral, Lund University, Sweden, Lund, 1997.
[12] A. Alfrey, E.F. Gurnee, W.G. Lloyd, J. Polym. Sci. C12 (1966) 249.
[13] M.F. Mills, R.G. Gilbert, D.H. Napper, Macromolecules 23 (1990) 4247.
[14] M.C. Piton, R.G. Gilbert, B.E. Chapman, P.W. Kuchel, Macromolecules 26 (1993) 4472.
[15] P.A.G.M. Scheren, D.T. Russell, D.F. Sangster, R.G. Gilbert, A.L. German, Macromolecules 28 (1995) 3637.
[16] D.T. Russel, R.G. Gilbert, D.H. Napper, Macromolecules 26 (1993) 3538.
[17] R.G. Gilbert, Emulsion Polymerization. A Mechanistic Approach, Academic Press, London, 1995, pp. 36–37, 116–120.

[18] P.-G. d. Gennes, Scaling Properties in Polymer Physics, Cornell University, Ithaca NY, New York, 1979, pp. 223–230.
[19] G.V.Z. Schultz, Phys. Chem. (Frankfurt am Main) 8 (1956) 290.
[20] L. Ivarsson, O. Karlsson, D.C. Sundberg, Work in progress.
[21] S.K. Soh, Diffusion Controlled Vinyl Polymerization, PhD Thesis, University of New Hampshire, Durham, NH, 1981.
[22] I.A. Maxwell, B.R. Morrison, D.H. Napper, R.G. Gilbert, Macromolecules 24 (1991) 1629.
[23] S. Shen, M.S. El-Aasser, V.L. Dimone, J.W. Vanderhoff, E.D. Sudol, J. Polym. Sci.: Part A: Polym. Chem. 29 (1991) 857.
[24] J.-E. Jönsson, H. Hassander, B. Törnell, Macromolecules 27 (1994) 1932.
[25] C.-S. Chern, G.W. Poehlein, J. Polym. Sci.: Part A: Polym. Chem. 25 (1987) 617.
[26] C.A. Croxton, M.F. Mills, R.G. Gilbert, D.H. Napper, Macromolecules 26 (1993) 3563.
[27] J.-E. Jönsson, Production of Two-Phase Latex Particles by Seeded Emulsion Polymerization — Polymerization Conditions and Particle Morphology, Doctoral Thesis, Lund Institute of Technology, Lund, 1994.
[28] J. Brandrup, E.H. Immergut (Eds.), Polymer Handbook, Wiley, New York, 1989, p. 1175.